THE JOURNAL OF PHYSICAL CHEMISTRY A
A JOURNAL OF THE AMERICAN CHEMICAL SOCIETY

pubs.acs.org/JPCA

Article

Millimeter-Wave and High-Resolution Infrared Spectroscopy of the Ground and Seven Lowest Fundamental States of 1*H*-1,2,4-Triazole

Hayley A. Bunn, Maria A. Zdanovskaia, Brant E. Billinghurst, Jianbao Zhao, Susanna L. Widicus Weaver, R. Claude Woods, Robert J. McMahon, and Brian J. Esselman*

Cite This: *J. Phys. Chem. A* 2024, 128, 6927−6942

Read Online

ACCESS | Metrics & More | Article Recommendations | Supporting Information

ABSTRACT: A combined analysis of millimeter-wave (70−700 GHz) and rotationally resolved infrared (400−1200 cm^{-1}) spectra of the ground state and seven fundamental vibrational modes of 1*H*-1,2,4-triazole is reported. While the lowest-energy vibrationally excited state (ν_{18}) is well-treated using a single-state distorted-rotor Hamiltonian, the second (ν_{17}) and third (ν_{16}) vibrationally excited states are involved in strong *c*-type Coriolis coupling and require an appropriate two-state Hamiltonian. The oblate nature of 1*H*-1,2,4-triazole is sufficiently close to the oblate symmetric-top limit that the analysis requires the use of A-reduced, sextic centrifugally distorted-rotor Hamiltonian models in the I^r representation in order to achieve low σ_{fit} values. The coupling between ν_{17} (A″) and ν_{16} (A″) resulted in many transitions with slightly perturbed frequencies, many highly displaced resonant intrastate transitions, and 165 nominal interstate transitions. Modeling the spectra of ν_{17} and ν_{16} required three *c*-axis Coriolis-coupling terms (F_{ab}, F^J_{ab}, and F^K_{ab}) to treat the interaction. Many of the nominal interstate transitions form clearly discernible Q-branch bands, comprising degenerate sets of *a*- and *b*-type transitions. The rotational spectra of four higher-energy vibrationally excited states (ν_{15}, ν_{14}, ν_{13}, and ν_{12}), which form a complex polyad involving Coriolis and anharmonic coupling interactions, were analyzed by single-state models, thus producing only effective spectroscopic constants. Inclusion of rotationally resolved infrared transitions enabled the accurate and precise determination of vibrational band origins for the four lowest-energy fundamental states: ν_{18} = 542.601 824 3 (28) cm^{-1}, ν_{17} = 665.183 128 5 (43) cm^{-1}, ν_{16} = 682.256 910 5 (43) cm^{-1}, and ν_{15} = 847.557 400 (11) cm^{-1}.

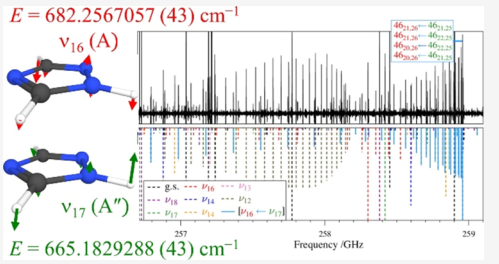

INTRODUCTION

Triazoles (c-$C_2H_3N_3$) are five-membered aromatic rings containing three nitrogen atoms. The differing arrangement of nitrogen atoms results in two regioisomers (1,2,3-triazole and 1,2,4-triazole) that can each exist in two tautomeric forms (Figure 1). The most stable triazole isomer in the gas phase is 1*H*-1,2,4-triazole (C_s), which is lower in energy by 6.25, 13.5, and 17.5 kcal/mol than 4*H*-1,2,4-triazole (C_{2v}), 2*H*-1,2,3-triazole (C_{2v}), and 1*H*-1,2,3-triazole (C_s), respectively, at the CCSD(T)/CBS level.[1] 1*H*- and 2*H*-1,2,3-Triazole have been observed using rotational spectroscopy[2−6] and high-resolution infrared (IR) spectroscopy.[6] While both 1*H*- and 4*H*-1,2,4-triazole are lower in energy than both 1,2,3-triazole tautomers, only the more stable tautomer of 1,2,4-triazole has been observed using gas-phase spectroscopy.[7−11] The exclusive observation of the 1*H*-1,2,4-triazole tautomer (Figure 2) is due to a combination of factors. 1,2,4-Triazole has a very low vapor pressure (0.0972 Pa or 0.73 mTorr at 21 °C),[12] making it more difficult to observe either 1,2,4-triazole tautomer than either tautomer of the more volatile 1,2,3-triazole. Additionally, the energy separation between the tautomers of 1,2,4-triazole is larger by 2 kcal/mol than that of 1,2,3-triazole,[1] thereby substantially reducing the population of the higher-energy tautomer. Finally, the more stable tautomer of 1,2,4-triazole

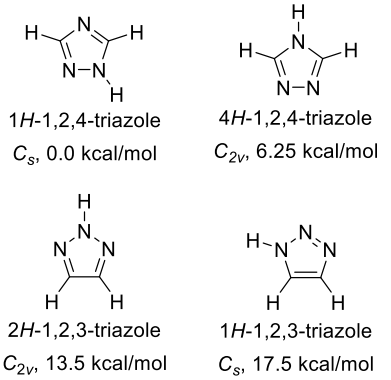

Figure 1. Triazole isomers with symmetry point groups and relative energies (kcal/mol) at the CCSD(T)/CBS level.[1]

Received: June 11, 2024
Revised: July 24, 2024
Accepted: July 25, 2024
Published: August 9, 2024

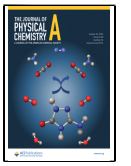

https://doi.org/10.1021/acs.jpca.4c03890
J. Phys. Chem. A 2024, 128, 6927−6942

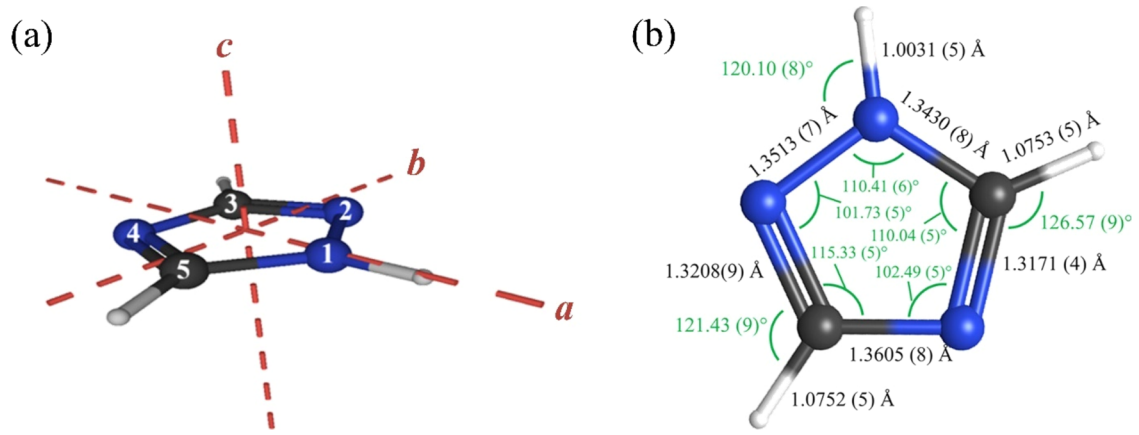

Figure 2. (a) 1*H*-1,2,4-Triazole ($C_2H_3N_3$, C_s, μ_a = 0.810 (90) D, μ_b = 2.579 (60) D, κ = 0.824)[7] with principal inertial axes and atom numbering. (b) Semi-experimental equilibrium structure (r_e^{SE}) with 2σ statistical uncertainties.[11]

Table 1. Previously Reported Infrared Assignments of the Seven Lowest-Energy Fundamental States of 1*H*-1,2,4-Triazole

Mode [a]	Sym	Bougeard[10] 1976 gas	Kudchadker[13] 1973 condensed	Movshovich[14] 1981 [b] condensed	Billes[15] 2000 condensed
ν_{18}	A″	538	640		550
ν_{17}	A″	652 [c]	660	645	649
ν_{16}	A″	678	693	682	681
ν_{15}	A″	842	885	891	884
ν_{14}	A″	883	990	934	926
ν_{13}	A′	957 [c]	930	971	955
ν_{12}	A′	970	965	985	980

[a]Consistent color codes are used for the fundamental modes in all tables and figures. [b]Assignments not given, but inferred by Billes *et al.*[15] [c]Condensed-phase value reported.

has a much larger dipole moment than the more stable tautomer of 1,2,3-triazole.[4,7] Using microwave spectroscopy (15−26 GHz), the spectroscopic constants,[7−9] dipole moment,[7] nuclear quadrupole coupling constants,[8] and r_0 structure[9] of 1*H*-1,2,4-triazole were reported in the early 1970s. Recently, the observed rotational spectra for these three isomeric triazoles (1*H*-1,2,4-, 1*H*-1,2,3-, and 2*H*-1,2,3-) and their isotopologues have been extended into the millimeter-wave frequency range (up to 375 GHz for 1,2,3-triazole and 700 GHz for 1,2,4-triazole) leading to precise and accurate semi-experimental equilibrium (r_e^{SE}) structure determinations.[5,11] A combined millimeter-wave and high-resolution infrared spectroscopy study analyzed the low-energy vibrational states of 1*H*- and 2*H*-1,2,3-triazole.[6] The current work provides an investigation of the vibrationally excited states of 1*H*-1,2,4-triazole, as no experimental spectroscopic constants or fundamental frequencies determined by high-resolution infrared spectroscopy have been reported.

Low-resolution gas- and condensed-phase infrared[10,13−15] and Raman[10,13,15] spectra have previously been reported up to 4000 cm^{-1} for 1*H*-1,2,4-triazole, providing estimates of the vibrational band origins (Table 1). Several discrepancies, however, exist between the vibrational assignments of the spectra presented in these previous works for the A″ vibrational modes. Assignments of the lowest-energy fundamental band origin (ν_{18}) vary by 102 cm^{-1}. Movshovich *et al.*[14] and Billes *et al.*[15] place the band origin at 538 and 550 cm^{-1}, respectively, while Kudchadker *et al.*[13] assigned it at 640 cm^{-1}. This absorption at 640 cm^{-1} that Kudchadker *et al.*[13] assigned to ν_{18} appears to correspond to the 645 and 649 cm^{-1} absorptions assigned to ν_{17} by Movshovich *et al.*[14] and Billes *et al.*,[15] respectively. Bougeard *et al.*[10] did not observe ν_{17} in their gas-phase study, but did report a condensed-phase value of 652 cm^{-1}. Likewise, Kudchadker *et al.*[13] reported an infrared signal at 660 cm^{-1}, and they assigned this signal to ν_{17}. Though the experimental frequencies vary by up to 15 cm^{-1}, the previous infrared studies agree on the assignments of ν_{16} (678−693 cm^{-1}).[10,13−15] All of the condensed-phase studies are in general agreement on the assignment of ν_{15} (885−891 cm^{-1}),[13−15] while Bougeard *et al.* assigned ν_{15} at 842 cm^{-1} in their gas-phase study.[10] The absorption at 883 cm^{-1} was assigned to ν_{14} in this same study,[10] while the other studies concluded that the state ∼885 cm^{-1} was ν_{15}.[13−15] Similar discrepancies are observed in the assignments of the A′ modes.

In this work, we use complementary analysis of the high-resolution infrared and millimeter-wave rotational spectra to disentangle the vibrational assignments and precisely determine the band origins for ν_{18}, ν_{17}, ν_{16}, and ν_{15} of 1*H*-1,2,4-triazole. To this end, we provide least-squares fits of the rotational and rotationally resolved infrared transitions for these vibrationally excited states, including an in-depth analysis of the Coriolis coupling between ν_{17} and ν_{16}.

EXPERIMENTAL METHODS

The millimeter-wave measurements of 1,2,4-triazole have been reported previously[11] and were acquired using a previously described millimeter-wave spectrometer.[11,16] In brief, a commercial sample of 1,2,4-triazole (97%) was heated to

https://doi.org/10.1021/acs.jpca.4c03890
J. Phys. Chem. A 2024, 128, 6927−6942

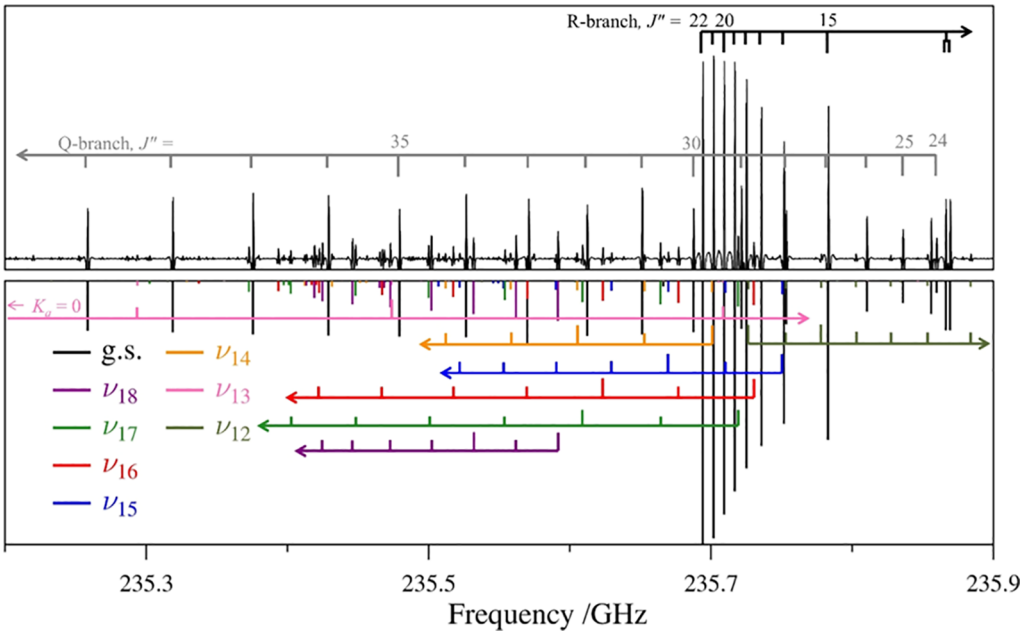

Figure 3. Experimental rotational spectrum (top) showing the J'' = 22 *b*-type R-branch bands of 1*H*-1,2,4-triazole from 235.2 to 235.9 GHz and stick spectra (bottom) from experimental spectroscopic constants with the ground state (black), ν_{18} (purple), ν_{17} (green), ν_{16} (red), ν_{15} (blue), ν_{14} (orange), ν_{13} (pink), and ν_{12} (olive). R-branch arrows indicate the direction of decreasing J'' from the K_a = 0 transitions for each state. Q-branch transitions of the ground state are indicated in gray for the K_c'' = 24 series. Unlabeled transitions are attributed to higher-energy vibrationally excited states and heavy-atom isotopologues.

~100 °C and introduced into a 2-m, stainless-steel cell (~100 °C) with a sample pressure of approximately 15 mTorr. Continuous broadband spectra were collected from 70 to 700 GHz with a 0.1 MHz step size. Heating the cell was necessary throughout the data collection due to the low volatility of 1,2,4-triazole.[12]

Infrared spectra of 1*H*-1,2,4-triazole were collected at the Canadian Light Source (CLS), on the Far-Infrared beamline, using a Bruker IFS 125 HR FTIR spectrometer equipped with a KBr beamsplitter and a pulsed-tube cooled Ge/Cu detector. A White-type multipass gas cell was used with a 30-cm base path length and a total optical path length of 7.2 m. In an approach inspired by previous work at CLS on imidazole,[17] the cell was heated using three Tempco silicone rubber heaters, which were made to enclose the cell. Each heater was controlled with a separate controller; two were controlled with Digi-Sense 68900−01 controllers and one with an Omega CN401 controller. Temperatures were measured using thermocouples built into the heaters. 1*H*-1,2,4-Triazole was loaded into a copper sample vessel, which was placed inside the gas cell. The gas cell was then pumped down to below 0.001 Torr, and background scans were collected. The cell was subsequently sealed and heated to ~100 °C. Scans were collected with a resolution of 0.00096 cm^{-1} and a mirror velocity of 80 kHz (measured as the frequency of laser modulation). The final spectrum was an average of 118 scans processed using the room-temperature background scan.

The rotational and high-resolution infrared spectra were analyzed using Kisiel's Assignment and Analysis of Broadband Spectra (AABS) software.[18,19] Pickett's SPFIT and SPCAT programs[20] were used for least-squares fitting and spectral predictions, along with Kisiel's PIFORM, PLANM, and AC programs for analysis.[21] All least-squares fitting output files are provided in the Supporting Information.

COMPUTATIONAL METHODS

An electronic structure calculation of 1*H*-1,2,4-triazole was carried out with Gaussian 16[22] using the WebMO interface[23] to obtain theoretical spectroscopic constants. The optimized geometry at the B3LYP/6-311+G(2d,p) level was obtained using "verytight" convergence criteria and an "ultrafine" integration grid, and a subsequent anharmonic vibrational frequency calculation was carried out. Additional electronic structure calculations were carried out using a development version of CFOUR[24] to obtain an optimized structure at the CCSD(T)/cc-pCVTZ level of theory. The optimized geometry and the same level of theory were subsequently used for an anharmonic, second-order vibrational perturbation theory (VPT2) calculation, wherein cubic force constants are evaluated by numerical differentiation of analytic first derivatives at displaced points.[25−27] These calculations provided fundamental frequencies, vibration−rotation interaction constants, and centrifugal distortion constants. Computational output files can be found in the Supporting Information.

RESULTS AND DISCUSSION

Rotational Spectrum. 1*H*-1,2,4-Triazole is a near-oblate (κ = 0.824) asymmetric top of C_s symmetry with both *a*- and *b*-axis dipole moment components (μ_a = 0.810 (90) D, μ_b = 2.579 (60) D).[7] Its ground-state rotational spectrum has pronounced *b*-type transitions and much weaker *a*-type transitions, as seen in Figure S1. Spectral collection at ~100 °C resulted in enhanced relative intensities of transitions with higher J/K quantum numbers in the ground vibrational-state and of the vibrationally excited-state transitions relative to those of the ground vibrational state. At 700 GHz, some series of *b*-type transitions have not even reached their peak intensity. Altogether, many thousands of rotational transitions were

https://doi.org/10.1021/acs.jpca.4c03890
J. Phys. Chem. A 2024, 128, 6927−6942

Table 2. Experimental and Computational Spectroscopic Constants for the Ground and Three Lowest-Energy Vibrationally Excited States of 1*H*-1,2,4-triazole (A-Reduced Hamiltonian, I^r Representation)

	ground state		ν_{18} (A″, 543 cm^{-1}) [a]	ν_{17} (A″, 665 cm^{-1}) [a]	ν_{16} (A″, 682 cm^{-1}) [a]
	CCSD(T) [b]	Experimental	Experimental	Experimental	Experimental
A_v (MHz)	10220.8	10245.082 967 (43)	10223.222 910 (80)	10221.339 428 (90)	10218.845 342 (93)
B_v (MHz)	9760.6	9832.081 172 (40)	9809.453 676 (70)	9798.563 658 (83)	9803.188 485 (90)
C_v (MHz)	4990.3	5015.129 951 (45)	5013.348 820 (58)	5016.331 946 (73)	5016.549 319 (73)
Δ_J (kHz)	2.009	2.064 424 (23)	2.067 216 (42)	2.022 081 (44)	2.029 250 (46)
Δ_{JK} (kHz)	−0.782	−0.858 933 (52)	−0.846 86 (17)	−0.789 59 (17)	−0.659 43 (18)
Δ_K (kHz)	2.278	2.346 844 (60)	2.323 35 (18)	2.355 14 (21)	2.095 89 (23)
δ_J (kHz)	0.807	0.830 584 5 (58)	0.830 234 (18)	0.808 743 (19)	0.812 493 (21)
δ_K (kHz)	1.357	1.374 545 (16)	1.367 087 (49)	1.258 423 (56)	1.344 368 (59)
Φ_J (Hz)	0.000 790	0.000 798 6 (37)	0.000 818 (10)	0.000 539 3 (68)	0.000 630 5 (71)
Φ_{JK} (Hz)	−0.000 251	−0.000 316 (17)	−0.000 381 (34)	[−0.000 316] [c]	[−0.000 316] [c]
Φ_{KJ} (Hz)	−0.005 43	−0.005 503 (28)	−0.006 54 (20)	−0.001 459 (42)	−0.002 489 (42)
Φ_K (Hz)	0.006 20	0.006 304 (12)	0.007 60 (28)	0.001 541 (34)	0.002 128 (34)
ϕ_J (Hz)	0.000 397	0.000 396 42 (94)	0.000 409 0 (49)	0.000 268 9 (34)	0.000 326 1 (37)
ϕ_{JK} (Hz)	0.000 455	0.000 420 5 (59)	[0.000 420 5] [c]	[0.000 420 5] [c]	[0.000 420 5] [c]
ϕ_K (Hz)	0.002 98	0.003 065 2 (42)	0.002 715 (96)	[0.003 065 2] [c]	[0.003 065 2] [c]
E_v (MHz)			16266793.463 (83)	19941688.51 (13)	20453547.62 (13)
E_v (cm^{-1})			542.601 824 3 (28)	665.183 128 5 (43)	682.256 910 5 (43)
F_{ab} (MHz)				4.770 838 (24)	
$F_{ab}{}^J$ (MHz)				−0.000 040 762 (32)	
$F_{ab}{}^K$ (MHz)				0.000 077 433 (73)	
Δ_i (uÅ^2) [d]	0.048 7	0.040 917 (1)	−1.473 28 (1)	−0.273 643 (2)	−0.265 744 (2)
κ [e]	0.824	0.842	0.841	0.838	0.840
N_{lines} (rot) [f]		4434 [g]	2925	2697	2497
N_{lines} (IR) [f]			1909		1341
σ_{fit} rot (MHz)		0.033	0.034	0.041	0.041
σ_{fit} IR (MHz)			3.2		4.6

[a]Experimental fundamental frequencies when available (*vide infra*) or CCSD(T)-computed frequencies. [b]Evaluated with the cc-pCVTZ basis set. [c]Values in brackets held constant at their corresponding ground-state values. [d]Inertial defect, $\Delta_i = I_c - I_a - I_b$, calculated using PLANM from the B_v constants. [e]$\kappa = (2B - A - C)/(A - C)$ [f]Number of independent transitions. [g]Includes transitions reported by all previous works.[7−9,11]

measured, assigned, and least-squares fit to the ground and seven lowest-energy vibrationally excited states.

Ground Vibrational State. The rotational spectrum of 1*H*-1,2,4-triazole has been analyzed previously using A- and S-reduced, sextic centrifugally distorted-rotor Hamiltonians in the III^r representation.[11] The *b*-type, R-branch transitions that dominate the rotational spectrum form typical oblate-type band structures (Figure 3). The ground state was previously analyzed using both A and S reductions in the III^r representation; the σ_{fit} value for the A-reduction least-squares fit (0.041 MHz) was somewhat larger than that of the S-reduction least-squares fit (0.033 MHz). In that previous work, the A-reduction least-squares fit did not satisfactorily determine a complete set of sextic centrifugal distortion constants. It is possible that the slightly higher σ_{fit} value for the A-reduction, III^r-representation least-squares fit arises, in part, because the ϕ_J, ϕ_{JK}, and ϕ_K constants are held constant at their CCSD(T) computed values. Both the inability to determine these off-diagonal sextic centrifugal distortion constants and the higher σ_{fit} value may also indicate that the A-reduced Hamiltonian is beginning to break down. A breakdown of the A-reduced Hamiltonian was noted in the previous study for the ground vibrational state of the [1,3-^{2}H]-1*H*-1,2,4-triazole isotopologue (κ = 0.975).[11] With a smaller κ value of 0.8421 for the ground vibrational state of the normal isotopologue of 1*H*-1,2,4-triazole, a breakdown of the A-reduced Hamiltonian was not initially anticipated or previously identified. The new least-squares fit presented in this work, like that obtained using the S reduction and III^r representation,[11] could be successfully employed to determine a complete set of sextic centrifugal distortion constants and a σ_{fit} value of 0.033 MHz (Table 2). The quality of the least-squares fit is improved when the representation or reduction is changed (the two standard methods of accounting for the A-reduced Hamiltonian breakdown),[11,28−33] indicating that the A-reduced Hamiltonian in the III^r reduction is not adequately modeling all measured transitions for the normal isotopologue. This type of breakdown is discussed further for the analysis of the Coriolis-coupled dyad of ν_{17} and ν_{16}, where the choice of representation becomes even more critical (*vide infra*).

The values predicted at the CCSD(T)/cc-pCVTZ level of theory are overall in excellent agreement with the experimental spectroscopic constants of the 1*H*-1,2,4-triazole vibrational ground state. The rotational constants are predicted within 1% of the experimental values. Interestingly, both the quartic and sextic centrifugal distortion constants are within 3% of the experimental values, with the exceptions of Δ_{JK}, Φ_{JK}, and ϕ_{JK} (which have absolute deviations of 9, 21, and 8%, respectively). Comparison to the B3LYP-predicted constants is provided in the Supporting Information.

Vibrationally Excited States. Initial prediction and assignment of the rotational spectra of the vibrationally excited states was made from the experimental ground-state spectroscopic constants with the rotational constants adjusted

https://doi.org/10.1021/acs.jpca.4c03890
J. Phys. Chem. A 2024, 128, 6927−6942

by computed vibration−rotation interaction constants ($B_0 - B_v$). This approach was effective for quickly assigning, measuring, and least-squares fitting the rotational transitions using Loomis-Wood plots. The stick spectra were repredicted and additional transitions added until all transitions that could be accurately measured across the frequency range were included in the data set. When high-resolution infrared data became available for ν_{18}, ν_{16}, and ν_{15}, rotationally resolved infrared transitions were added to the data set, providing the information to determine a precise and accurate vibrational energy. In each least-squares fit where high-resolution infrared transitions were used, the ground-state spectroscopic constants were held at their previously determined values.

In 1*H*-1,2,4-triazole, all of the A″ fundamentals are lower in energy than all the A′ fundamentals. The lowest-energy vibrationally excited state, ν_{18} (A″, 542.6 cm^{-1}, Figure 4),

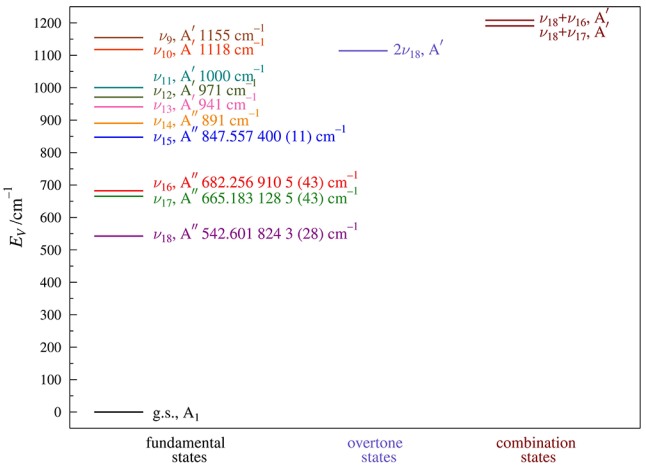

Figure 4. Vibrational energy levels of 1*H*-1,2,4-triazole below 1200 cm^{-1}. The energy values for ν_{18}, ν_{17}, ν_{16}, and ν_{15} result from the experimental analysis presented herein. All other vibrational frequencies were computed at the CCSD(T)/cc-pCVTZ level. Consistent color codes are used for the fundamental modes in all tables and figures.

corresponding to a ring deformation mode with a large out-of-plane N−H bend (Figure 5), is well-isolated from the other vibrational states and can be adequately modeled as a single-state distorted rotor. In contrast, ring deformation modes ν_{17} (A″, 665.2 cm^{-1}) and ν_{16} (A″, 682.3 cm^{-1}) are sufficiently close in energy that their spectra are strongly perturbed by a mutual *c*-type Coriolis interaction. The lower-energy vibration (ν_{17}) is characterized by large N−H and C2−H out-of-plane motions, while the higher-energy vibration (ν_{16}) is largely a C4−H out-of-plane motion. These three vibrationally excited states are the main focus of the subsequent analysis; each state is modeled with an appropriate sextic centrifugally distorted-rotor Hamiltonian model with a low σ_{fit} value. Rotational transitions for several additional vibrational states (ν_{15}, ν_{14}, ν_{13}, and ν_{12}), as well as high-resolution infrared transitions for ν_{15}, have been measured, assigned, and least-squares fit. These states form a complex Coriolis- and anharmonic-coupled polyad, likely involving additional vibrational states whose spectra have not been conclusively assigned. Therefore, due to the extent of these coupling interactions that cannot be adequately addressed at present, effective fits that include relatively unperturbed transitions for the fundamental states up to ν_{12} (A′, 971 cm^{-1}) are provided in this work.

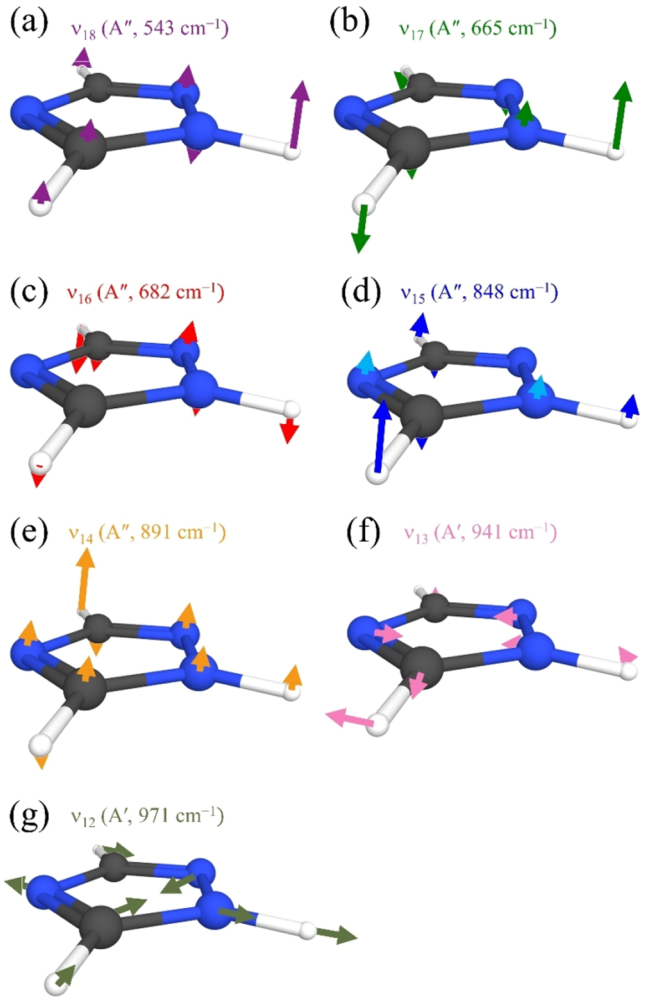

Figure 5. Vibrational modes, symmetries, and frequencies for ν_{18} through ν_{12}. The energy values for ν_{18}, ν_{17}, ν_{16}, and ν_{15} result from the experimental analysis presented herein, whereas ν_{14}, ν_{13}, and ν_{12} use computed energy values (CCSD(T)/cc-pCVTZ). Consistent color codes are used for the fundamental modes in all tables and figures.

Spectral Analysis of ν_{18}. The lowest-energy fundamental state, ν_{18} (A″, 542.6 cm^{-1}), has a typical near-oblate asymmetric-top rotational spectrum, including strong R-branch bands, consisting of transitions with two intense *b*-type ($^{b}R_{1,1}$, $^{b}R_{-1,1}$) and two weaker *a*-type ($^{a}R_{0,1}$) components, separated by ∼2*C*. In contrast to the ground state,[11] the bands of ν_{18} and the other A″ modes initially progress to lower frequency with increasing *J* values (Figure 3), due to the negative inertial defects of each state (Table 2). Weaker Q-branch transitions are also observed throughout the spectrum, again with two *b*-type ($^{b}Q_{1,-1}$) and two *a*-type components ($^{a}Q_{2,-1}$, $^{a}Q_{0,-1}$), many of which are degenerate. The large number of assigned transitions of ν_{18} and their distribution in J'' and K_a'' are shown in Figure S2 (rotational) and Figure S3 (infrared). In total, over 2900 rotational and 1900 infrared transitions, with maximum J'' and K_a'' values of 83 and 50, respectively, have been least-squares fit to a single-state, sextic distorted-rotor Hamiltonian model in the A reduction, I^r representation (σ_{fit} = 0.034 MHz). The resulting rotational and centrifugal distortion constants, as well as the vibrational energy, are provided in Table 1. Comparison of the quartic and sextic centrifugal distortion constants of ν_{18} to their corresponding ground-state

https://doi.org/10.1021/acs.jpca.4c03890
J. Phys. Chem. A 2024, 128, 6927−6942

Table 3. Vibration-Rotation Interaction Constants of Vibrationally Excited States of 1*H*-1,2,4-Triazole

	Experimental	B3LYP [a]	*obs.* − *calc.*	CCSD(T) [b]	*obs.* − *calc.*
$A_0 - A_{18}$ (MHz)	21.860 057 (91)	21.56	0.30	22.28	−0.42
$B_0 - B_{18}$ (MHz)	22.627 496 (81)	22.05	0.58	22.29	0.34
$C_0 - C_{18}$ (MHz)	1.781 131 (73)	1.41	0.37	1.66	0.12
$A_0 - A_{17}$ (MHz)	23.743 54 (10)	23.37	0.37	22.45	1.29
$B_0 - B_{17}$ (MHz)	33.517 14 (92)	33.92	−0.41	33.19	0.33
$C_0 - C_{17}$ (MHz)	−1.201 995 (86)	−1.24	0.04	−1.21	0.01
$A_0 - A_{16}$ (MHz)	26.237 62 (10)	26.67	−0.43	27.68	−1.44
$B_0 - B_{16}$ (MHz)	28.892 687 (98)	28.95	−0.06	27.82	1.07
$C_0 - C_{16}$ (MHz)	−1.419 368 (86)	−1.46	0.04	−1.27	−0.15
$A_0 - A_{15}$ (MHz)	15.949 48 (21)	15.20	0.75	15.98	−0.03
$B_0 - B_{15}$ (MHz)	24.641 66 (18)	23.47	1.17	24.00	0.64
$C_0 - C_{15}$ (MHz)	−1.711 05 (17)	−2.09	0.38	−1.79	0.08
$A_0 - A_{14}$ (MHz)	11.775 29 (10)	11.13	0.65	11.77	0.01
$B_0 - B_{14}$ (MHz)	38.867 43 (19)	38.74	0.13	39.28	−0.41
$C_0 - C_{14}$ (MHz)	−0.729 98 (18)	−1.02	0.29	−0.70	−0.03
$A_0 - A_{13}$ (MHz)	−14.874 52 (31)	−15.59	0.71	−16.00	1.12
$B_0 - B_{13}$ (MHz)	−12.784 60 (33)	−13.38	1.05	−13.43	0.65
$C_0 - C_{13}$ (MHz)	30.450 04 (16)	32.01	−1.56	29.41	1.04
$A_0 - A_{12}$ (MHz)	−0.822 44 (31)	−0.39	−0.43	−1.54	0.72
$B_0 - B_{12}$ (MHz)	−16.533 67 (30)	−17.42	0.89	−18.10	1.57
$C_0 - C_{12}$ (MHz)	−0.851 13 (19)	−2.44	1.59	−1.89	1.04

[a]Evaluated with the 6-311+G(2d,p) basis set. [b]Evaluated with the cc-pCVTZ basis set.

values shows the expected small deviations. The deviations are less than 1.5% for the quartic terms and 21% for the sextic terms, except for ϕ_{JK} and ϕ_K which could not be determined satisfactorily and were therefore held constant at their ground-state values. The computed vibration−rotation interaction constant values (Table 3) are in excellent agreement with their experimental values (0.42 MHz or ∼2% for $A_0 - A_{18}$, 0.34 MHz or ∼1.5% for $B_0 - B_{18}$, and 0.12 MHz or ∼7% for $C_0 - C_{18}$). The agreement of these vibration−rotation interaction and centrifugal distortion constants with the computed and ground-state values, respectively, provides confirmation of the quality of the least-squares fits and the adequacy of the treatment of ν_{18} as a single-state distorted rotor.

The infrared spectrum of ν_{18} (A″) consists of a relatively intense *c*-type band at 542.601 824 3 (28) cm^{-1}, shown in Figure 6. As the rotationally resolved infrared transitions were added to the data set after least-squares fitting the rotational transitions, the IR assignments were only a one-parameter problem requiring manual adjustment of the ν_{18} energy value in the initial spectral prediction. The least-squares fit utilizes the ground-state spectroscopic constants held at their values determined in this work. The previous energy value of ν_{18} of 538 cm^{-1} with low-resolution gas-phase infrared spectroscopy[10] is in good agreement with the more precise and accurate value reported herein.

Spectral Analysis of ν_{17} and ν_{16}. The second- and third-lowest energy fundamental states, ν_{17} and ν_{16}, are separated by only 17 cm^{-1}, thus their energy levels experience significant state-mixing *via* Coriolis coupling. This interaction results in substantial perturbations in the observed rotational-transition frequencies and prevents each state from being adequately treated as a single-state distorted rotor. Initially, the rotational spectra of ν_{17} and ν_{16} were approached as single-state distorted rotors, per the method described above. After assigning a few K_a series, it became apparent that neither of these vibrationally excited states could be adequately modeled without treating Coriolis coupling between states. These single-state least-squares fits resulted in several spectroscopic constants showing large, nearly equal and opposite deviations from their ground-state values, along with curving series and significant gaps in Loomis-Wood plots. Both ν_{17} and ν_{16} have A″ symmetry, enabling interactions *via* symmetry-allowed *c*-axis Coriolis coupling or anharmonic coupling. Both vibrational modes are out-of-plane motions, causing the corresponding Coriolis-coupling constant ($\zeta^c_{17,16}$) to be zero. Therefore, the proper treatment of Coriolis interaction between these states is expected to involve the second-order Coriolis coefficient, F_{ab}, and its centrifugal distortion expansion terms. Only a very

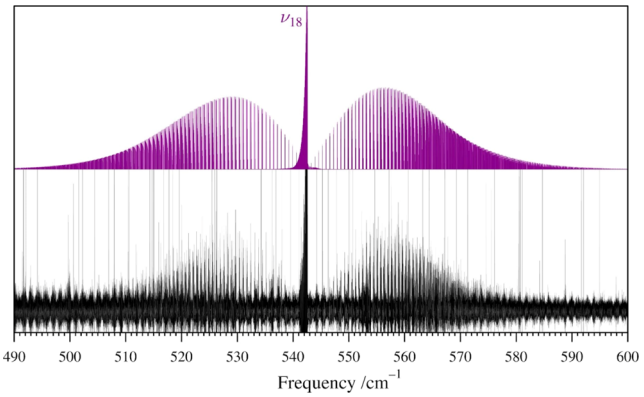

Figure 6. Predicted stick spectrum of ν_{18} (purple, top) and the experimental high-resolution infrared spectrum (bottom) of 1*H*-1,2,4-triazole from 490 to 600 cm^{-1}.

https://doi.org/10.1021/acs.jpca.4c03890
J. Phys. Chem. A 2024, 128, 6927−6942

small G_c value is possible, which can arise via contributions from higher-order G_c terms. The interaction between these out-of-plane ring deformations (ν_{17} and ν_{16}) of 1*H*-1,2,4-triazole is analogous to those previously observed in other aromatic heterocycles such as furan (ν_{14} and ν_{11})[34,35] and pyridazine (ν_{16} and ν_{13}),[36] which were well-modeled with the appropriate F terms.

Based upon the previous work,[11] these states were initially treated using a sextic, centrifugally distorted, A-reduced Hamiltonian in the III^r representation matching the original ground-state analysis. As additional perturbed transitions were added to the data set one K_a series at a time, coupling terms were allowed to vary. Although the global perturbations present throughout the rotational spectrum enabled a preliminary estimate of the coupling, the energy separation and initially determined coupling terms were unable to predict resonances. Therefore, it was necessary to employ a technique wherein a resonance was identified as a gap in a Loomis-Wood plot and the energy separation was manually adjusted until a resonance became predicted at the appropriate J values. Allowing the energy separation and coupling terms to fit with this closer estimate enabled the least-squares fit to determine the values more accurately and to better predict the highly perturbed resonant and nominal interstate transitions. Incorporation of such transitions into the data set produced a fully predictive fit. A substantial effort was made to confirm the assignment of each transition using Loomis-Wood plots and resonance plots. Additionally, we conducted a thorough exploration of various combinations of Coriolis-coupling and anharmonic-coupling terms, and which centrifugal distortion constants were allowed to vary. Despite these efforts, we were unable to obtain a converging, low-error least-squares fit. At this point, we began to suspect that the difficulty in obtaining a converged least-squares fit could be associated with the use of the III^r representation of the Hamiltonian model.

To address the coupling between two states such as ν_{17} and ν_{16}, we employ the standard c-axis Coriolis-coupling terms, G_c^J, G_c^K, F_{ab}^J, F_{ab}^K, F_{ab}^{JJ}, F_{ab}^{JK}, *etc.*, which are intrinsically A-reduction Coriolis constants, in either the I or III representation. Switching the representation of the least-squares fit of the dyad from the III^r to I^r almost immediately resulted in a converged, low-error fit (σ_{fit} = 0.041 MHz for each state) using just three coupling terms: F_{ab}, F_{ab}^J, and F_{ab}^K. The change in representation of the dyad fit necessitated the corresponding change in representation for the ground-state least-squares fit. In addition to the reasons described above, the ground-state constants in the I^r representation are needed to provide meaningful comparison for their vibrationally excited-state centrifugal distortion constants and appropriate values at which to hold excited-state constants that cannot be determined. The need to change representation was initially unexpected, as the κ values for both ν_{17} (0.838) and ν_{16} (0.840) are similar to κ values of many other species that are in fact reasonably well treated with an A-reduced Hamiltonian in either representation. It is not clear if the change in reduction for the vibrationally excited states addressed unhelpful correlations between centrifugal distortion and Coriolis-coupling coefficients, better modeled the centrifugal distortion, or both. In any event, this switch of reduction did enable a satisfactory converged least-squares fit (low σ_{fit} value, physically meaningful constants, and predictive of the observable spectrum).

The resulting spectroscopic constants from the Coriolis-coupled least-squares fit of ν_{17} and ν_{16} are provided in Table 2. The rotational constants show only small changes relative to their corresponding ground-state values. The vibration–rotation interaction constants (Table 3) for these states show excellent agreement between their computed and experimental values. This situation is typical where the least-squares fit adequately treats the Coriolis coupling, and in particular for cases like this one, where the interacting states do not have a Coriolis ζ and corresponding large G term. The quartic centrifugal distortion constants vary by less than 25% from their ground-state values. Only a partial set of sextic distortion constants were determined, and these constants show deviations of up to 63% relative to their ground-state values. Efforts to hold these large-deviation constants at their ground-state values increased the σ_{fit} values and resulted in many transitions rejected from the fit, so the constants were allowed to vary in the least-squares fit. Importantly, none of the spectroscopic constants exhibit the near-equal magnitude but opposite sign deviation with respect to their ground-state values, a phenomenon that would be characteristic of incorporation of Coriolis-coupling into the centrifugal distortion constants. The large observed changes are likely due to an inadequate data set for ν_{17} and ν_{16} leading to an incomplete treatment of the centrifugal distortion and the necessity of holding some sextic parameters constant at their ground-state values.

As noted by Bougeard *et al.*[10] and predicted using the computed electric dipole moment vibrational matrix elements, ν_{17} has a very small infrared intensity and was not observed in the previous or current gas-phase infrared spectra. Nevertheless, the frequency of ν_{17} is very well determined in the current work as a consequence of the detailed analysis of the Coriolis coupling of ν_{17} and ν_{16}, analysis of the rotational spectra of both states, and the analysis of the infrared spectrum of ν_{16} shown in Figure 7. Importantly, the dataset consists of many substantially perturbed, resonant, and nominal interstate rotational transitions for both vibrationally excited states, which enables such complete treatment of the Coriolis interaction and precise and accurate determination of the energy separation between the two states. Thus, the vibrational frequency of ν_{17} is determined with comparable precision and accuracy to that of ν_{16} from the combination of the latter's vibrational frequency and the energy separation between the two states.

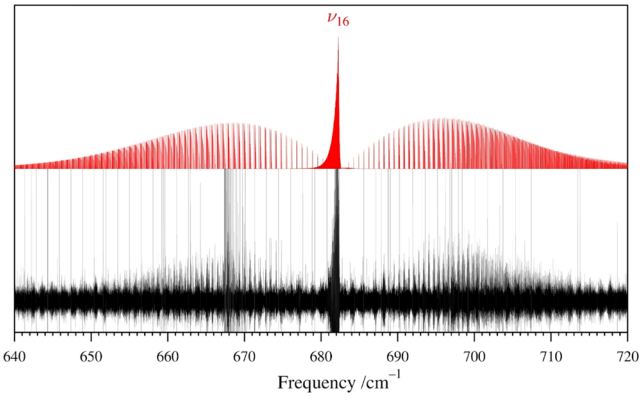

Figure 7. Predicted stick spectrum of ν_{16} (red, top) and the experimental high-resolution infrared spectrum (bottom) of 1*H*-1,2,4-triazole from 640 to 720 cm^{-1}.

https://doi.org/10.1021/acs.jpca.4c03890
J. Phys. Chem. A 2024, 128, 6927−6942

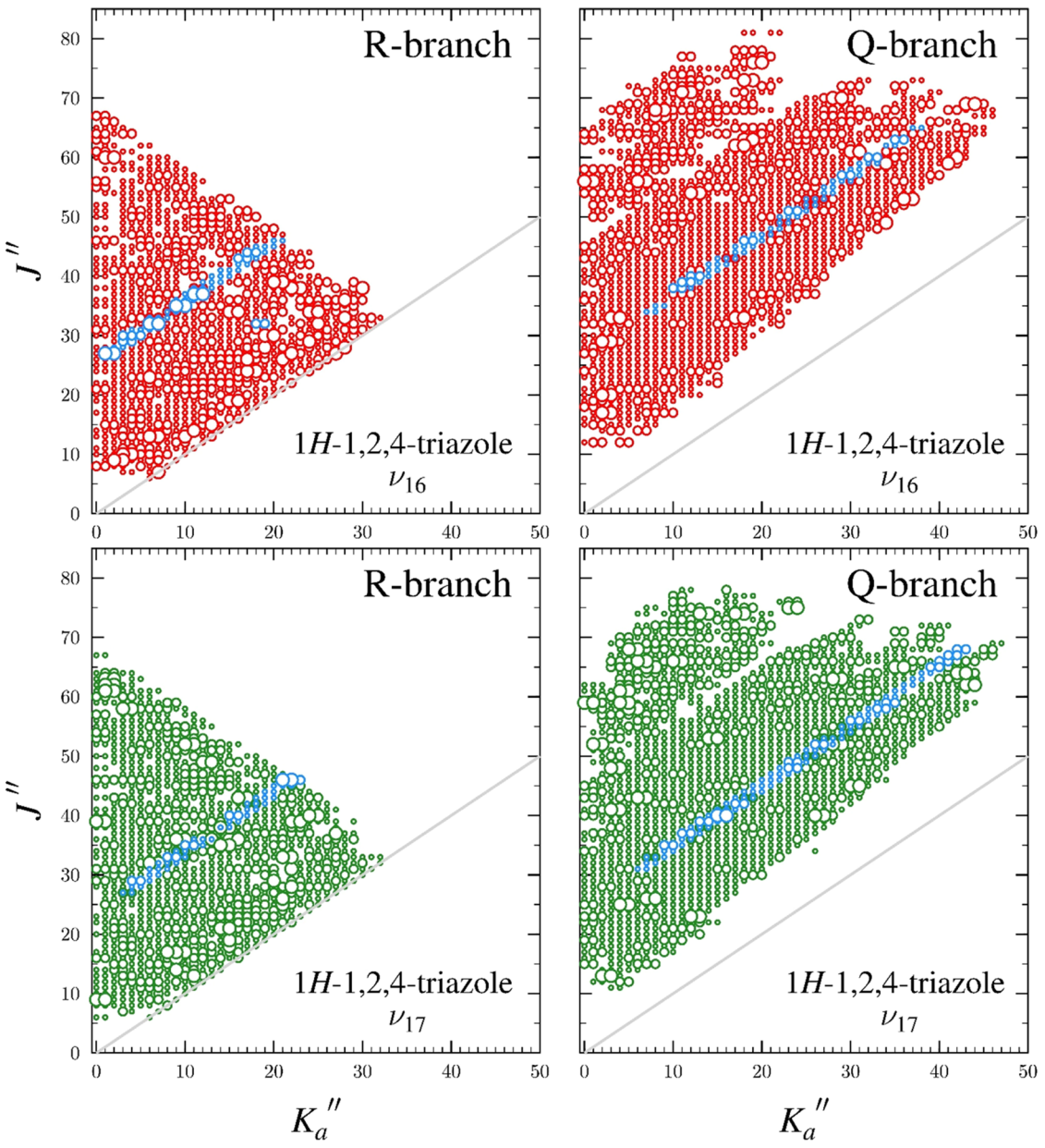

Figure 8. Data distribution plots for the least-squares fit of millimeter-wave spectroscopic data for 1*H*-1,2,4-triazole, ν_{17} (green, bottom) and ν_{16} (red, top). Light-blue circles indicate nominal interstate transitions whose lower-energy level belongs to the state labeled in the plot. The size of the outlined circle is proportional to the value of $|(f_{obs.} - f_{calc.})/\delta f|$, where δf is the frequency measurement uncertainty, and where δf is the nominal frequency measurement uncertainty (50 kHz), and all values of the ratio represented are smaller than 3.

The final transition data set includes over 2650 rotational transitions for ν_{17} and 2450 rotational transitions for ν_{16}, with an additional 1340 rotationally resolved *c*-type IR transitions for ν_{16}. While insufficient to determine a complete set of sextic centrifugal distortion constants, as shown in Figures 8 (rotational) and S4 (IR), each vibrational state has an extensive data set covering a large range of J and K_a values that can all be fit with low *obs.* − *calc.* values. The J'' quantum-number values range from 6 to 78 and 6 to 88 for ν_{17} and ν_{16}, respectively. The K_a'' quantum-number values range from 0 to 47 and 0 to 46 for ν_{17} and ν_{16}, respectively. The most striking features in these data distribution plots are the large diagonal groups of nominal interstate transitions. There are 90 nominal interstate transitions with the lower-energy rotational level in ν_{17} and 75 nominal interstate transitions with the lower-energy rotational level in ν_{16}. These transitions are very well modeled, having *obs.* − *calc.* values similar to any of the intrastate transitions.

The corresponding resonances observed in many of the R-branch and Q-branch series of ν_{17} and ν_{16} conform to *c*-type selection rules (ΔK_a = odd, ΔK_c = even) for the Coriolis interactions. As shown in the multi-K_a series resonance progression plot of Figure 9a, the R-branch ν_{17} K_a series show small resonances as low as K_a = 2, which steadily increase in intensity and progress to higher J values with increasing K_a. At K_a = 20, the displacement of the resonant transition has risen to approximately 2.7 GHz from its expected frequency, absent local perturbation; nevertheless, this transition is successfully included in the least-squares fit. The large undulations that occur at low-J portions of the K_a series,

https://doi.org/10.1021/acs.jpca.4c03890
J. Phys. Chem. A 2024, 128, 6927−6942

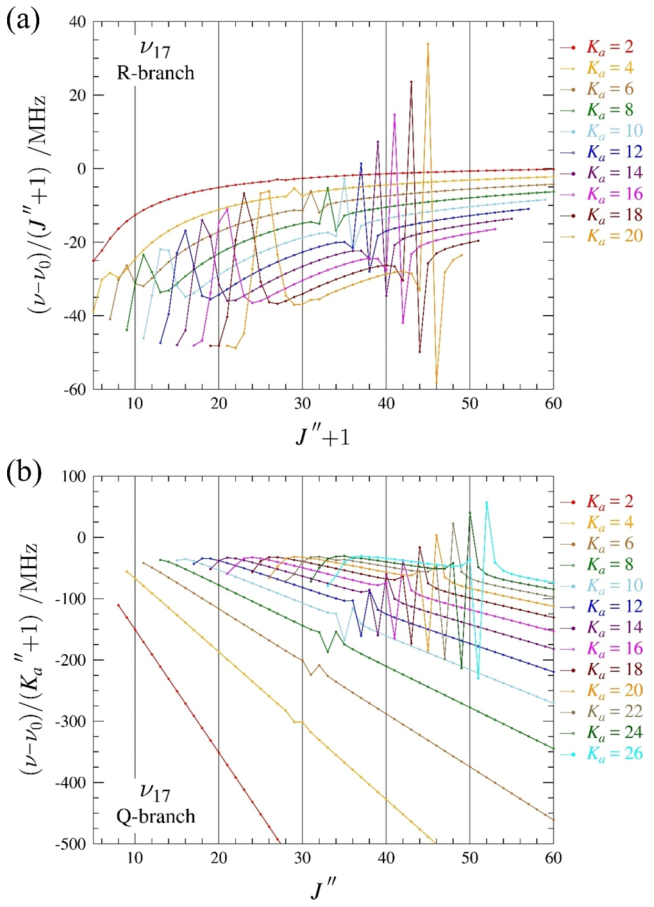

Figure 9. Superimposed resonance plots of ν_{17} (a) R-branch, *b*-type transitions for K_a^+ series from 2 to 20 and (b) Q-branch, *b*-type transitions for K_a^- series from 2 to 26 for 1*H*-1,2,4-triazole. Measured transitions are omitted for clarity, but they are indistinguishable from the plotted values on this scale. The plotted values are frequency differences between excited-state transitions and their ground-state counterparts, scaled by $(J'' + 1)$ or $(K_a'' + 1)$ values for the R- and Q-branch transitions, respectively.

which occur in the region of J values where the behavior transitions from near-prolate top to near-oblate top, also increase in intensity and progress to higher J values as K_a increases. Figure 9b displays an analogous multi-K_a series resonance plot for the Q-branches of ν_{17}. The Q-branches show the same resonances, beginning as low as $K_a = 2$ that similarly increase in intensity and progress to higher J values as K_a increases. The frequency of the resonant transition in the $K_a = 26$ series is perturbed by approximately 10.2 GHz. This transition is not included in the data set because it is overlapping with a more intense transition from a different species. The most-perturbed R-branch transition included in the data set for ν_{17} is displaced by ∼2.8 GHz, while the most-perturbed Q-branch transition is displaced by ∼11.8 GHz.

A total of 165 symmetry-allowed, nominal interstate transitions between ν_{17} and ν_{16} have been measured, assigned, and incorporated into the least-squares fit. These *a*- and *b*-type transitions areformally allowed by symmetry as difference-band transitions between ν_{17} and ν_{16}. They only become observable in 1*H*-1,2,4-triazole, however, near strong resonances, due to state mixing and borrowed intensity from their corresponding intrastate transitions. Figure 10 shows the relationship between matched pairs of observed nominal interstate and intrastate transitions between ν_{17} and ν_{16}. The moderate size of the resonances in the K_a series corresponds to a moderate amount of intensity transfer, allowing both the inter- and intrastate transitions to have sufficient intensity to be observed. The measurement of all four of the transitions in the matched pairs shown in Figure 10 (left) allows a completely experimental confirmation of their correct assignment. As they share the same four energy levels, the difference between the average frequencies of the interstate and intrastate transition should be zero. For the set of transitions displayed in Figure 10, this difference is 0.011 MHz, which is substantially less than the nominal measurement uncertainty of 0.050 MHz.

One of the nominal interstate transitions (ν_{16} $41_{15,27} \leftarrow \nu_{17}$ $40_{17,24}$ in Figure 10) is part of an R-branch series that can be seen in the Loomis-Wood plot shown in Figure 11. For a range of 20 K_a values, the state-mixing between ν_{17} and ν_{16} is sufficiently intense to produce an entire series of nominal interstate transitions. The only exceptions occur in a region of very low signal intensity, which arises due to a hardware limitation and is not inherent to the spectrum, or where there are much larger overlapping transitions from other vibrational states. These nominal interstate transitions are associated with the diagonal blue group of transitions in Figure 8 and indicate the crossing of many energy levels between ν_{16} and ν_{17}. An analogous Loomis-Wood plot can be made showing the corresponding series of R-branch nominal interstate transitions from $\nu_{17} \leftarrow \nu_{16}$.

In a highly unusual feature, the spectrum includes Q-branch bands of nominal interstate transitions ($\nu_{16} \leftarrow \nu_{17}$ or $\nu_{17} \leftarrow \nu_{16}$), which comprise degenerate sets of *a*- and *b*-type transitions. These bands are in contrast to the more typical cases of sporadic R- and Q-branch nominal interstate transitions occurring independently throughout the spectral range. One of these Q-branch series is depicted in Figure 12, where the Q-branch transitions share a constant value of K_c (K_c = 25 of ν_{17} in the lower state and K_c = 26 of ν_{16} in the upper state). The apparent bandhead at about 258.96 GHz is a turnaround of transitions in the band, which starts with observable transitions at J'' = 31 (258.1 GHz) and increases in frequency with increasing J''. At J'' = 46 (highlighted in Figure 12), the series turns around and progresses to lower frequency with further increases in J''. Each of the nominal interstate transitions in the Q-branch has a lower-energy level associated with one of the highly perturbed resonant transitions from an intrastate Q-branch band. Figure 13 shows the relationship between two resonant transitions whose lower-state energy levels are strongly mixing. This mixing results in the perturbation of the associated interstate Q-branch transitions by about 7 GHz and the appearance of strong nominal interstate transitions. The interaction of many energy levels associated with Q-branch transitions in this J/K region gives rise to the band structure observed in Figure 12.

All of the perturbed transitions and nominal interstate transitions provide critical information about the Coriolis coupling and energy difference between ν_{17} and ν_{16}. Combined with the high-resolution infrared transitions of ν_{16}, highly precise and accurate vibrational frequencies are determined for each state: ν_{17} = 665.183 128 5 (43) cm^{-1} and ν_{16} = 682.256 910 5 (43) cm^{-1}. The frequency of ν_{16} reported by Bougeard *et al.*[10] of 678 cm^{-1}, obtained with low-resolution infrared spectroscopy, is in reasonable agreement with its updated value.

https://doi.org/10.1021/acs.jpca.4c03890
J. Phys. Chem. A 2024, 128, 6927−6942

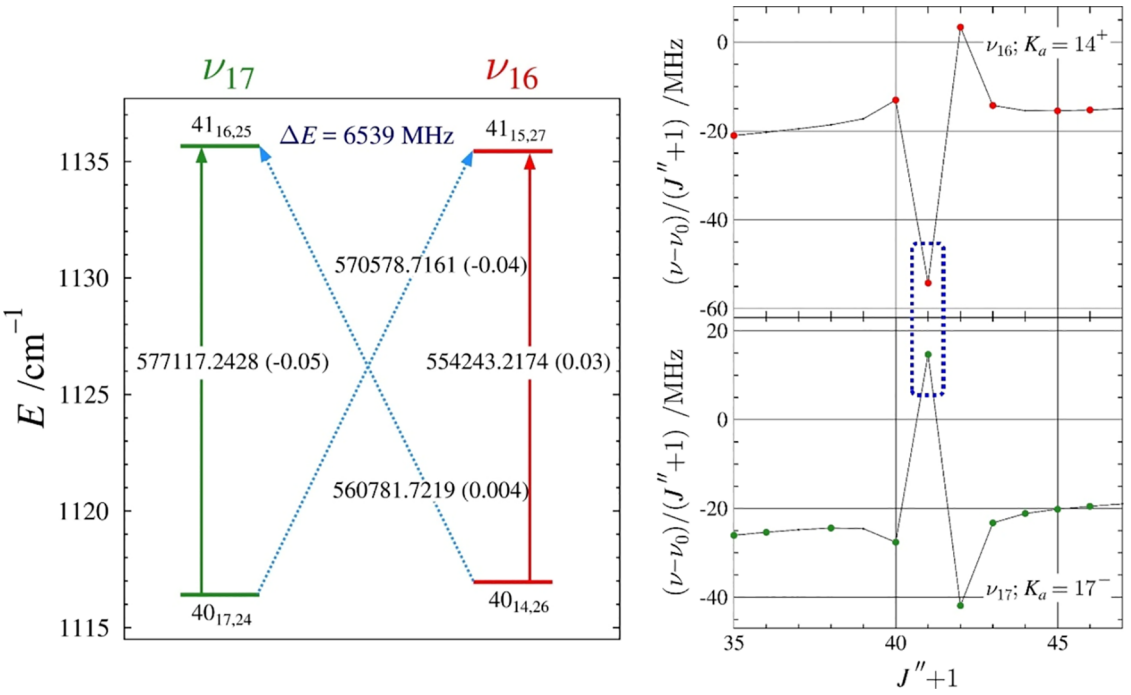

Figure 10. Energy diagram (left) depicting a representative matched pair of R-branch nominal interstate transitions between the ν_{17} (green) and ν_{16} (red) vibrational states of 1*H*-1,2,4-triazole. Standard *b*-type transitions within vibrational states are denoted by vertical arrows. The diagonal, dashed light-blue arrows indicate nominal interstate transitions that are formally forbidden, but enabled because of rotational energy-level mixing. Values printed on each of the arrows are the corresponding transition frequency (in MHz) with its *obs.* − *calc.* value in parentheses. The marked energy separation is between the two strongly interacting rotational energy levels. Resonance plots (right) of the K_a series of ν_{17} and ν_{16} that contain the corresponding resonant in-state transitions are denoted by a blue box.

The values of the spectroscopic constants for this dyad permit a straightforward explanation of the perturbation behavior between ν_{17} and ν_{16}. The vast majority of the nominal interstate transitions and highly perturbed resonant transitions occur within a narrow range of J/K energy levels (Figure 8). The resonance plots shown in Figure 9 (along with the smoothly interleaving ones for odd K_a values or those beyond K_a = 26 − not shown) cover almost the entire quantum number range of our experiments and thus show the most perturbed intrastate transitions that are observable in the frequency range. Each of the Q-branch resonances in Figure 9b shares one of the same rotational energy levels as the R-branch resonances in Figure 9a. The magnitudes of the frequency shifts appear different because of (1) the different vertical scales between the two plots and (2) the differences in the Coriolis perturbation experienced by the other pair of the energy levels involved in the respective R- and Q-branch transitions. The signs of the frequency shifts are inverted because the rotational energy-levels cross in the upper state of the transition in the R-branch transitions and in the lower state in the Q-branch transitions (Figures 10 and 13). The Loomis-Wood plot in Figure 11 displays the nominal interstate transitions that have a common lower energy level with the most frequency-shifted in-state (ν_{17}) series of transitions in Figure 9a. Several similar Loomis-Wood plots could be made for ν_{17}, though with fewer observable transitions for the nearby series that correspond to slightly less perturbed in-state transitions producing less intense interstate transitions (less state mixing), *e.g.*, J'' increased by one for the same K_a in Figure 9a. It is clear from inspection of Figure 9 that the strong resonances appear fairly separated from the undulations and are therefore in the range of K_c values corresponding to normal oblate-top behavior. Although we have shown that the I^r representation produces better convergence in the least-squares fit, the III^r representation is much more appropriate for explaining approximate behavior in this range of K_c values. The rigid-rotor Hamiltonian

$$(\mathcal{H}_{rr} = AP_a^2 + BP_b^2 + CP_c^2)$$

rearranges to

$$\mathcal{H}_{rr} = \frac{A+B}{2}P^2 + \left(C - \frac{A+B}{2}\right)P_c^2 + \left(\frac{A-B}{2}\right)(P_a^2 - P_b^2)$$

In the III^r representation, where K_c is the eigenvalue of P_c, this Hamiltonian has diagonal elements $\left(\frac{A+B}{2}\right)J(J+1)$ and $\left(C - \frac{A+B}{2}\right)K_c^2$ and off-diagonal elements proportional to $(A - B)$. The off-diagonal, or asymmetry, terms have a small effect in this range (as indicated by the degeneracy of transitions with common K_c values) and can be ignored here. Also, because $(A + B)$ is almost the same in the two perturbing states, the first term almost cancels when calculating the unperturbed energy separation between two states with a Coriolis interaction (ΔJ = 0). This unperturbed energy separation is also the energy denominator in a second-order perturbation theory treatment of the Coriolis perturbation. This unperturbed energy difference (ΔE) is thus approximated in zeroth order by eq 1 (using a ΔK_c = 2 selection rule).

https://doi.org/10.1021/acs.jpca.4c03890
J. Phys. Chem. A 2024, 128, 6927−6942

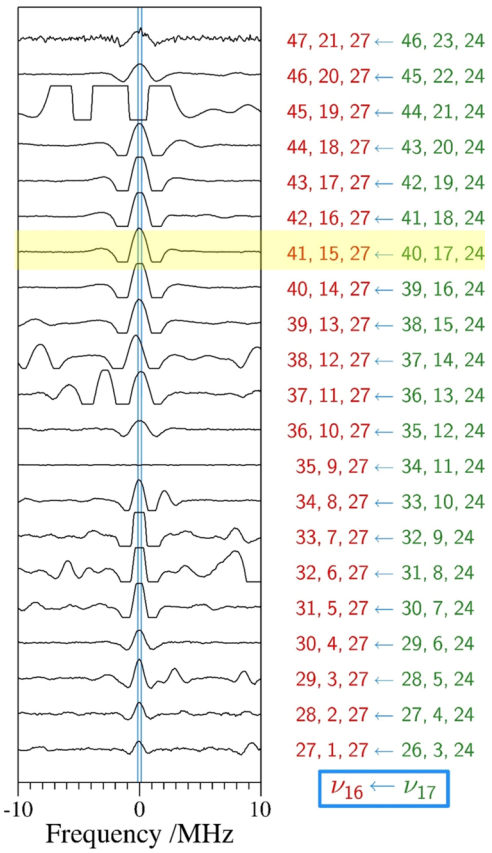

Figure 11. Loomis–Wood plot of nominal interstate transitions from ν_{17} (green) to ν_{16} (red) centered on the $K_c = 24^-$ series for ν_{17} ranging in J'' from 26 to 46. The transition corresponding to one of the nominal interstates depicted in Figure 10 is identified in yellow. Quantum numbers are provided for a single nominal interstate transition from a set of four degenerate transitions with the same constant K_c values.

$$\Delta E \cong E_{16} - E_{17} + \left(C - \frac{(A+B)}{2}\right)((K_c+2)^2 - K_c^2)$$
$$\cong 511\,859\ \text{MHz} - (4995\ \text{MHz})4(K_c+1)$$
$$\cong 7.6\ \text{GHz for}\ K_c = 25\ \text{in}\ \nu_{17} \quad (1)$$

For the actual case depicted in Figure 10 ($J'' + 1 = 41$, $K_a = 15$ in ν_{16}), this near-resonance computes to an energy separation of 4273 MHz when the centrifugal distortion and exact spectroscopic constants are taken into account. As J and K_a increase by one (holding K_c constant), the energy separation slowly decreases in the sequence 4035.9, 3788.1, 3529.8··· MHz. These relatively small energy separations enable sufficient interaction between the two vibrational states to produce the observed series of resonances whose intensities increase because of the combined effects of the decreasing energy separations and the increasing Coriolis matrix element dependent on F_{ab}. The energy separation reaches an actual zero-crossing between $J'' + 1 = 54$ and 55, which is just beyond the range shown in Figure 9b. In contrast, when K_c changes by one, holding $\Delta K_c = 2$ fixed, the unperturbed energy separation (second-order denominator) changes by about 19.98 GHz, drastically reducing the interaction and therefore the magnitude of the Coriolis frequency shift, the degree of state mixing, and the intensities of the corresponding interstate transitions.

Spectral Analysis of ν_{15}, ν_{14}, ν_{13}, and ν_{12}. The next four lowest-energy fundamental states (ν_{15}, ν_{14}, ν_{13}, and ν_{12}) of 1*H*-1,2,4-triazole are part of a complex Coriolis- and anharmonic-coupled polyad that may involve several additional vibrationally excited states (Figure 4). We measured, assigned, and least-squares fit transitions for each of the four above-listed states. We also have tentative assignments for several of the vibrationally excited states higher in energy than ν_{12}, but the weak intensities and complex coupling do not permit unambiguous assignments at this time. As a result, we present effective fits only for these four fundamental states for which transitions have been unambiguously assigned.

Over 1000 minimally perturbed millimeter-wave transitions have been included in the least-squares fits of each of the states, ν_{15}, ν_{14}, ν_{13}, and ν_{12}, using single-state distorted-rotor models, resulting in the spectroscopic constants presented in Table 4. For ν_{15}, 300 rotationally resolved, *c*-type IR transitions were included in the least-squares fit. This low number of transitions is due to the weak intensity of the IR band, and not due to the unaddressed coupling. Figure 14, which displays the experimental and predicted IR spectra of ν_{15}, shows that the signal-to-noise ratio for this band is much smaller than those for either ν_{18} or ν_{16}. As a result of the relatively small number of infrared transitions for ν_{15} and the lack of addressed coupling to a nearby state, the precision of the determined energy (847.554 00 (11) cm^{-1}) is slightly less than for ν_{18}, ν_{17}, and ν_{16}. No IR transitions could be measured for the higher-energy fundamental states. A weak feature at 888 cm^{-1}, however, is likely the *c*-type Q-branch of ν_{14}. For each of these fundamental states, the data set employed was limited to transitions that could reasonably be least-squares fit to a single-state, sextic distorted-rotor Hamiltonian in the A reduction and I^r representation. For each state, many transitions that are clearly assignable via Loomis-Woods plots have been excluded from the data set in order to achieve an effective fit with minimally perturbed constants. These effective fits of ν_{15}, ν_{14}, ν_{13}, and ν_{12} produced vibration–rotation interaction constants that are in reasonable agreement with their computed values (Table 3), comparable to the agreement between the computed and experimental vibration-rotation interaction constants for ν_{18}, ν_{17}, and ν_{16}. This provides a high level of confidence in the assignments of both the vibrational states and their transitions. The centrifugal distortion constants for these states show varying degrees of absorbed untreated coupling. All of the centrifugal distortion constants of ν_{15} seem to be reasonable compared to their corresponding ground-state values, suggesting that the spectroscopic constants for that state might be close to their true values. In contrast, the sextic centrifugal distortion constants of ν_{14} and ν_{13} show clear deviations from the corresponding ground-state values, indicating that they are absorbing a fair amount of untreated coupling. Thus, the values of Δ_{JK} and Δ_K and all of the sextic centrifugal distortions constants of ν_{12} are effective. Improvements to these constants would require, at a minimum, incorporation of the necessary Coriolis- and anharmonic-coupling terms between all involved states and would likely require additional assignments of rotationally resolved weak IR or Raman bands and inclusion of states whose rotational spectra have only been tentatively assigned.

Summary of the Infrared A″ Band Origins. While assignments of the vibrational band origins for 1*H*-1,2,4-triazole are available from previous low-resolution IR spectra, both in the gas- and condensed-phase, there are significant

https://doi.org/10.1021/acs.jpca.4c03890
J. Phys. Chem. A 2024, 128, 6927–6942

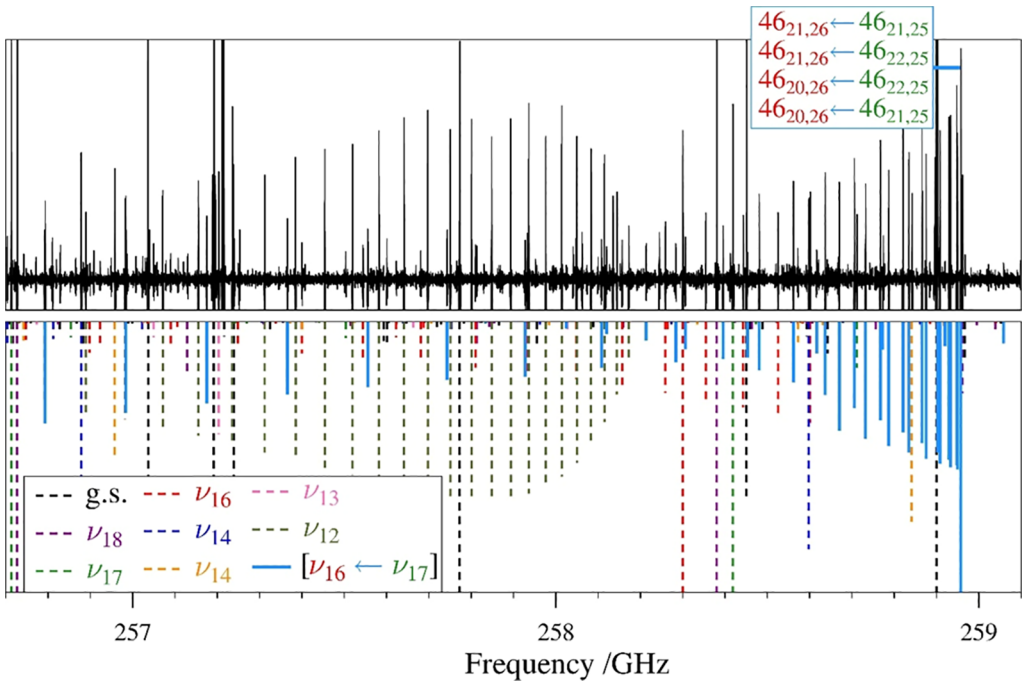

Figure 12. Experimental rotational spectrum (top) of 1*H*-1,2,4-triazole from 256.7 to 259.1 GHz and stick spectra (bottom) from experimental spectroscopic constants with the ground state (black, dashed), ν_{18} (purple, dashed), ν_{17} (green, dashed), ν_{16} (red, dashed), ν_{15} (blue, dashed), ν_{14} (orange, dashed), ν_{13} (pink, dashed), ν_{12} (olive, dashed), and $\nu_{16} \leftarrow \nu_{17}$ nominal interstate transitions (light blue, solid). The degenerate transitions for the intense peak of the apparent bandhead at 258.96 GHz are provided for reference.

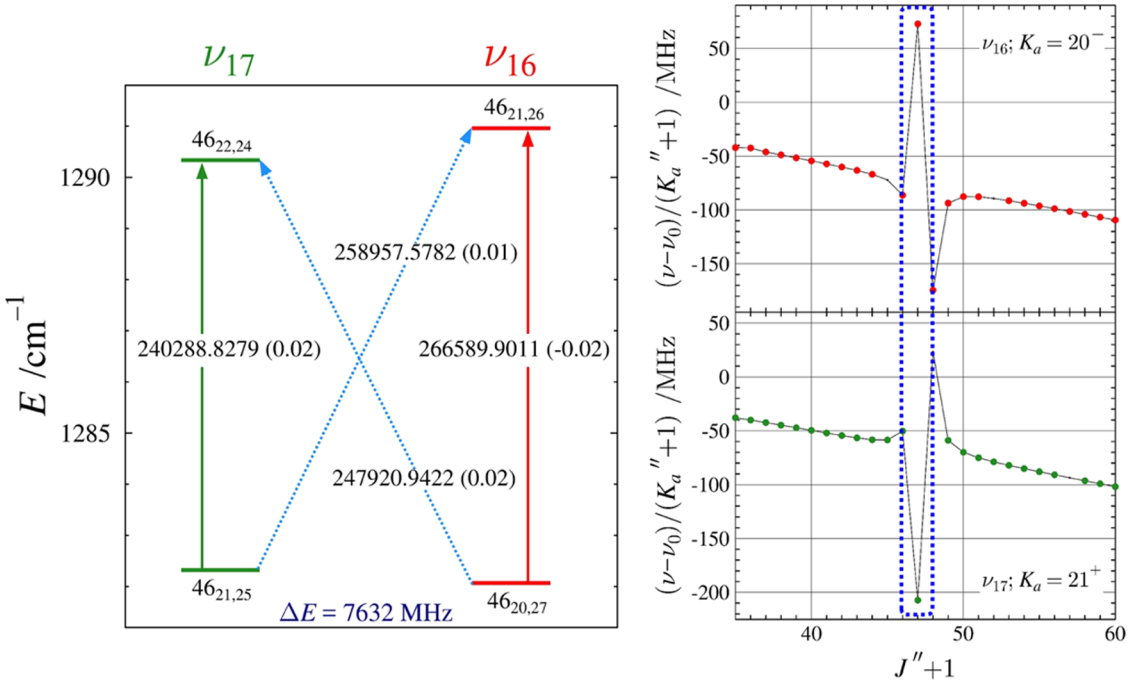

Figure 13. Energy diagram (left) depicting a representative matched pair of Q-branch nominal interstate transitions between the ν_{17} (green) and ν_{16} (red) vibrational states of 1*H*-1,2,4-triazole. Standard *b*-type transitions within vibrational states are denoted by vertical arrows. The diagonal, dashed light-blue arrows indicate nominal interstate transitions that are formally forbidden, but enabled because of rotational energy-level mixing. Values printed on each of the arrows are the corresponding transition frequency (in MHz) with its *obs.* − *calc.* value in parentheses. The marked energy separation is between the two strongly interacting rotational energy levels. Resonance plots (right) of the K_a series of ν_{17} and ν_{16} that contain the corresponding resonant in-state transitions denoted by a blue box.

discrepancies between their assignments.[10,13−15] The combined millimeter-wave and high-resolution infrared spectral analysis in this work resolves any ambiguity in the assignments of the four lowest-energy fundamental states. Only the gas-phase infrared analysis of Bougeard *et al.*[10] provides the correct vibrational state assignments (Table 5). It is unclear, however, why all of the vibrational frequencies reported in that low-resolution, gas-phase IR analysis are 4−5 cm^{-1} lower in energy

https://doi.org/10.1021/acs.jpca.4c03890
J. Phys. Chem. A 2024, 128, 6927−6942

Table 4. Experimental Spectroscopic Constants for the Ground Vibrational State and Effective Experimental Constants for Four Vibrationally Excited States of 1*H*-1,2,4-Triazole (A-Reduced Hamiltonian, I^r Representation)

	ground state Experimental	ν_{15} (A″, 848 cm^{-1}) [a] Experimental	ν_{14} (A″, 891 cm^{-1}) [b] Experimental	ν_{13} (A′, 941 cm^{-1}) [b] Experimental	ν_{12} (A′, 971 cm^{-1}) [b] Experimental
A_v (MHz)	10245.082 967 (43)	10229.133 49 (21)	10233.307 68 (21)	10259.957 49 (31)	10245.905 41 (31)
B_v (MHz)	9832.081 172 (40)	9807.439 51 (18)	9793.213 74 (19)	9844.865 77 (33)	9848.614 84 (30)
C_v (MHz)	5015.129 951 (45)	5016.841 00 (16)	5015.859 93 (17)	4984.679 91 (15)	5015.981 08 (18)
Δ_J (kHz)	2.064 424 (23)	2.013 99 (14)	1.916 63 (15)	1.975 97 (20)	2.384 06 (21)
Δ_{JK} (kHz)	−0.858 933 (52)	−0.776 75 (48)	−0.221 09 (57)	−0.472 0 (10)	−1.973 64 (82)
Δ_K (kHz)	2.346 844 (60)	2.256 66 (60)	1.723 07 (67)	2.234 9 (11)	3.213 42 (82)
δ_J (kHz)	0.830 584 5 (58)	0.805 239 (35)	0.757 283 (37)	0.943 783 (91)	0.820 929 (77)
δ_K (kHz)	1.374 545 (16)	1.252 83 (16)	1.108 35 (16)	1.504 97 (32)	1.687 67 (20)
Φ_J (Hz)	0.000 798 6 (37)	0.000 548 (30)	0.000 731 (35)	−0.006 674 (15)	0.009 911 (50)
Φ_{JK} (Hz)	−0.000 316 (17)	−0.000 533 (72)	−0.043 71 (22)	0.102 12 (17)	−0.065 75 (32)
Φ_{KJ} (Hz)	−0.005 503 (28)	[−0.005 50] [c]	0.179 76 (39)	−0.289 93 (39)	0.092 49 (60)
Φ_K (Hz)	0.006 304 (12)	[0.006 30] [c]	−0.169 42 (25)	0.226 04 (28)	−0.029 55 (44)
ϕ_J (Hz)	0.000 396 42 (94)	[0.000 396] [c]	[0.000 396] [c]	[0.000 396] [c]	[0.000 396] [c]
ϕ_{JK} (Hz)	0.000 420 5 (59)	[0.000 421] [c]	[0.000 421] [c]	[0.000 421] [c]	[0.000 421] [c]
ϕ_K (Hz)	0.003 065 2 (42)	[0.003 07] [c]	[0.003 07] [c]	[0.003 07] [c]	[0.003 07] [c]
E_v (MHz)		25409131.63 (34)			
E_v (cm^{-1})		847.557 400 (11)			
Δ_i (uÅ^2) [d]	0.0409 17(1)	−0.199 515 (3)	−0.234 512 (4)	0.794 763 (4)	0.114 068 (4)
κ [e]	0.842 1	0.838	0.831	0.843	0.848
N_{lines} (rot) [f]	4434	1328	1300	1183	1053
N_{lines} (IR) [f]		301			
σ_{fit} rot (MHz)	0.033	0.059	0.060	0.049	0.43
σ_{fit} IR (MHz)		4.43			

[a]Experimental fundamental frequency. [b]Computed frequency (CCSD(T)/cc-pCVTZ). [c]Values in brackets held constant at their corresponding ground-state values. [d]Inertial defect, $\Delta_i = I_c - I_a - I_b$, calculated using PLANM from the B_v constants. [e]$\kappa = (2B - A - C)/(A - C)$ [f]Number of independent transitions.

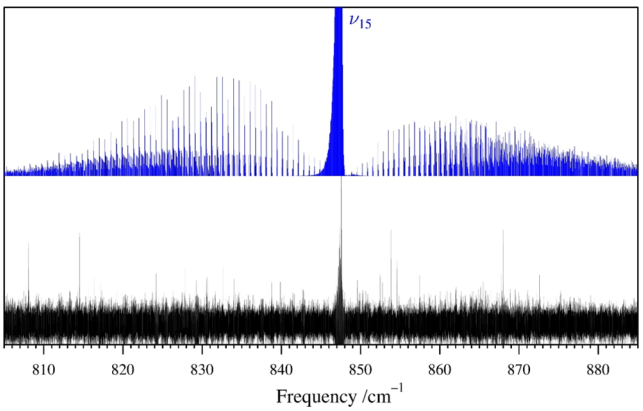

Figure 14. Predicted stick spectrum of ν_{15} (blue, top) and the experimental high-resolution infrared spectrum (bottom) of 1*H*-1,2,4-triazole from 805 to 885 cm^{-1}.

than those observed in this work. The computed fundamental frequencies at the CCSD(T)/cc-pCVTZ level are in excellent agreement (within 0.3 cm^{-1}) with our experimental values, except for ν_{18}, which differs by 12 cm^{-1}. The computed fundamental frequencies at the B3LYP/6-311+G(2d,p) level are generally in poorer agreement ($|obs. - calc.|_{avg}$ = 4.3 cm^{-1}) than the CCSD(T) values ($|obs. - calc.|_{avg}$ = 3.1 cm^{-1}), though each fundamental frequency is predicted by that method within 7 cm^{-1} of its experimental value.

This work provides an example of the synergy between millimeter-wave and high-resolution infrared spectroscopies applied to the same system, beyond the obvious facilitation of the IR assignment process when most of the spectroscopic constants are already well determined from the pure rotational analysis. The infrared intensity of 1*H*-1,2,4-triazole ν_{17} is too small to allow for straightforward measurement of its vibrational frequency *via* high-resolution infrared spectroscopy. This difficulty is further compounded by the very low vapor pressure of 1*H*-1,2,4-triazole. Transitions in the rotational spectrum of ν_{17}, however, can be assigned and measured in a very straightforward manner. Fortuitously, many of these transitions are perturbed by Coriolis coupling with ν_{16}, which has a sufficiently large infrared intensity to be observed by high-resolution infrared spectroscopy. It would be very challenging to address the coupling using the infrared data alone. The coupling is addressed very well using the rotational transitions given the very large number of transitions for both ν_{17} and ν_{16} perturbed by the interaction. As with many other cases, the interaction gives rise to new types of rotational transitions that provide information about their energy separation. As a result, the energy of ν_{17} is determined very precisely and accurately (to 0.000 004 cm^{-1}) *via* its coupling

https://doi.org/10.1021/acs.jpca.4c03890
J. Phys. Chem. A 2024, 128, 6927−6942

Table 5. Gas-Phase Experimental and Computed Vibrational Energies for the Seven Lowest-Energy Fundamental States of 1*H*-1,2,4-Triazole

	Exp this work	Exp Bougeard[10]	B3LYP [a]	*obs.* − *calc.* [b]	CCSD(T) [c]	*obs.* − *calc.* [b]
E_{18} (cm^{-1})	542.601 824 3 (28)	538	536.07	6.53	530.68	11.92
E_{17} (cm^{-1})	665.183 128 5 (43)		665.01	0.17	665.46	−0.28
E_{16} (cm^{-1})	682.256 910 5 (43)	678	686.62	−4.36	682.41	−0.15
E_{15} (cm^{-1})	847.557 400 (11)	842	841.31	6.25	847.47	−0.09
E_{14} (cm^{-1})	888 [d]	883	887.30		890.53	
E_{13} (cm^{-1})			949.57		941.10	
E_{12} (cm^{-1})		970	976.47		971.26	

[a]Evaluated with the 6-311G+(2d,p) basis set. [b]Observed values are those determined in this work. [c]Evaluated with the cc-pCVTZ basis set. [d]Tentative assignment.

with ν_{16} demonstrating the complementary nature of these techniques.

CONCLUSIONS

1*H*-1,2,4-Triazole is a moderately oblate (κ = 0.842) molecule whose ground-state rotational spectrum can be modeled using an A-reduced Hamiltonian with the oblate, III^r, representation seemingly well. Despite the ability to obtain an acceptably low-error least-squares fit, 1*H*-1,2,4-triazole is better treated with an A-reduced Hamiltonian in the I^r representation. This suggests that a generally good practice when working with the A-reduced Hamiltonian is to analyze the data set using both representations. That the representation issue can impact the behavior of a coupled dyad in the least-squares fitting process is particularly noteworthy. Even when the III^r representation seemed reasonable for the ground state and the κ values move only slightly further away from the oblate-top limit in the excited-state dyad (κ = 0.838 and 0.840 for ν_{17} and ν_{16}, respectively), the III^r representation can prevent the least-squares fitting of a data set to obtain a satisfactory or converging result.

Of particular note for the coupled dyad examined in this work are the nominal interstate R-branch and Q-branch transitions. In a somewhat unusual case, these transitions have sufficient intensity that entire bands or series of nominal interstate transitions are observable, rather than the more typical sporadic transitions. This fortunate circumstance can be well understood in terms of the approximate near-oblate-top quantum mechanics of 1*H*-1,2,4-triazole over a very wide range of quantum numbers studied in this work. These numerous nominal interstate transitions and the large number of in-state rotational transitions spanning a large frequency range are responsible for the precise and accurate determination of the energies of ν_{17} and ν_{16} and their Coriolis-coupling terms. These values provide useful benchmarks for future developments in computational chemistry, particularly in the prediction of higher-order Coriolis interactions.

ASSOCIATED CONTENT

Supporting Information

The Supporting Information is available free of charge at https://pubs.acs.org/doi/10.1021/acs.jpca.4c03890.

A-reduced Hamiltonian, I^r representation spectroscopic experimental and B3LYP constants of ground-state 1*H*-1,2,4-triazole; predicted stick spectrum of ground-state 1*H*-1,2,4-triazole; data set distribution plots for all other vibrationally excited states (PDF)

Computational output files; least-squares fitting files for all vibrational states (ZIP)

AUTHOR INFORMATION

Corresponding Author

Brian J. Esselman − *Department of Chemistry, University of Wisconsin−Madison, Madison, Wisconsin 53706, United States;* orcid.org/0000-0002-9385-8078; Email: esselman@wisc.edu

Authors

Hayley A. Bunn − *Department of Chemistry, University of Wisconsin−Madison, Madison, Wisconsin 53706, United States;* Present Address: Max Planck Institute for Extraterrestrial Physics, Garching 85748, Germany; orcid.org/0000-0002-7783-3049

Maria A. Zdanovskaia − *Department of Chemistry, University of Wisconsin−Madison, Madison, Wisconsin 53706, United States;* orcid.org/0000-0001-5167-8573

Brant E. Billinghurst − *Canadian Light Source. Inc., University of Saskatchewan, Saskatoon, Saskatchewan S7N 2 V3, Canada*

Jianbao Zhao − *Canadian Light Source. Inc., University of Saskatchewan, Saskatoon, Saskatchewan S7N 2 V3, Canada;* orcid.org/0000-0003-3864-2167

Susanna L. Widicus Weaver − *Department of Chemistry, University of Wisconsin−Madison, Madison, Wisconsin 53706, United States; Department of Astronomy, University of Wisconsin-Madison, Madison, Wisconsin 53706, United States;* orcid.org/0000-0001-6015-3429

R. Claude Woods − *Department of Chemistry, University of Wisconsin−Madison, Madison, Wisconsin 53706, United States;* orcid.org/0000-0003-0865-4693

Robert J. McMahon − *Department of Chemistry, University of Wisconsin−Madison, Madison, Wisconsin 53706, United States;* orcid.org/0000-0003-1377-5107

Complete contact information is available at: https://pubs.acs.org/10.1021/acs.jpca.4c03890

Notes

The authors declare no competing financial interest.

https://doi.org/10.1021/acs.jpca.4c03890
J. Phys. Chem. A 2024, 128, 6927−6942

■ ACKNOWLEDGMENTS

We thank Zbigniew Kisiel for thoughtful conversations about Coriolis coupling. We gratefully acknowledge funding from the U.S. National Science Foundation for support of this project (R.J.M., CHE-2245738 and CHE-1954270) and S.L.W.W.'s UW-Madison start-up fund. Part of the research described in this paper was performed at the Canadian Light Source, a national research facility of the University of Saskatchewan, which is supported by the Canada Foundation for Innovation (CFI), the Natural Sciences and Engineering Research Council (NSERC), the National Research Council (NRC), the Canadian Institutes of Health Research (CIHR), the Government of Saskatchewan, and the University of Saskatchewan.

■ REFERENCES

(1) Balabin, R. M. Tautomeric Equilibrium and Hydrogen Shifts in Tetrazole and Triazoles: Focal-Point Analysis and *ab initio* Limit. *J. Chem. Phys.* **2009**, *131*, No. 154307.
(2) Stiefvater, O. L.; Jones, H.; Sheridan, J. Double-Resonance-Double-Search Assignment of the Microwave Spectrum of 1,2,3-Triazole. *Spectrochim. Acta, Part A* **1970**, *26*, 825−833.
(3) Blackman, G. L.; Brown, R. D.; Burden, F. R.; Garland, W. Nuclear Quadrupole Coupling in the Microwave Spectrum of 1,2,3-Triazole. *J. Mol. Spectrosc.* **1977**, *65*, 313−318.
(4) Begtrup, M.; Nielsen, C. J.; Nygaard, L.; Samdal, S.; Sjørgen, C. E.; Sørensen, G. O. The Molecular Structure and Tautomer Equilibrium of Gaseous 1,2,3-Triazole Studied by Microwave Spectroscopy, Electron Diffraction and *Ab Initio* Calculations. *Acta Chem. Scand.* **1988**, *42a*, 500−514.
(5) Zdanovskaia, M. A.; Esselman, B. J.; Kougias, S. M.; Amberger, B. K.; Stanton, J. F.; Woods, R. C.; McMahon, R. J. Precise Equilibrium Structures of 1*H*- and 2*H*-1,2,3-Triazoles ($C_2H_3N_3$) by Millimeter-Wave Spectroscopy. *J. Chem. Phys.* **2022**, *157*, No. 084305.
(6) Zdanovskaia, M. A.; Franke, P. R.; Esselman, B. J.; Billinghurst, B. E.; Zhao, J.; Stanton, J. F.; Woods, R. C.; McMahon, R. J. Vibrationally excited states of 1*H*- and 2*H*-1,2,3-triazole isotopologues analyzed by millimeter-wave and high-resolution infrared spectroscopy with approximate state-specific quartic distortion constants. *J. Chem. Phys.* **2023**, *158*, No. 044301.
(7) Bolton, K.; Brown, R. D.; Burden, F. R.; Mishra, A. The Microwave Spectrum and Dipole Moment of 1,2,4-triazole: Identification of Tautomer in Vapour Phase. *J. Chem. Soc. D* **1971**, 873.
(8) Blackman, G. L.; Brown, R. D.; Burden, F. R.; Mishra, A. Quadrupole hyperfine structure of the microwave spectrum of 1,2,4-triazole and *N*-deuterotriazole. *J. Mol. Spectrosc.* **1975**, *57*, 294−300.
(9) Bolton, K.; Brown, R. D.; Burden, F. R.; Mishra, A. The Microwave Spectrum and Structure of 1,2,4-Triazole. *J. Mol. Struct.* **1975**, *27*, 261−266.
(10) Bougeard, D.; Le Calvé, N.; Roch, B. S.; Novak, A. 1,2,4-Triazole: Vibrational Spectra, Normal Coordinate Calculations, and Hydrogen Bonding. *J. Chem. Phys.* **1976**, *64*, 5152−5164.
(11) Bunn, H. A.; Esselman, B. J.; Franke, P. R.; Kougias, S. M.; McMahon, R. J.; Stanton, J. F.; Widicus Weaver, S. L.; Woods, R. C. Millimeter/Submillimeter-wave Spectroscopy and the Semi-Experimental Equilibrium (r_e^{SE}) Structure of 1*H*-1,2,4-Triazole (*c*-$C_2H_3N_3$). *J. Phys. Chem. A* **2022**, *126*, 8196−8210.
(12) Jiménez, P.; Roux, M. V.; Turrión, C. Thermochemical Properties of N-Heterocyclic Compounds II. Enthalpies of Combustion, Vapour Pressures, Enthalpies of Sublimation, and Enthalpies of Formation of 1,2,4-Triazole and Benzotriazole. *J. Chem. Thermodyn.* **1989**, *21*, 759−764.
(13) Kudchadker, S. A.; Rao, C. N. R. Infrared Spectra & Normal Vibrations of Isomeric Triazoles. *Indian J. Chem.* **1973**, *11*, 140−142.
(14) Movshovich, D. Y.; Sheinker, V. N.; Zayakina, T. A.; Garnovskii, A. D.; Osipov, O. A. Study of the Structure and Properties of Heterocyclic Compounds and Their Complexes. XLVII. Vibrational Spectra and Structure of Complexes of 1,2,4-Triazole and 1-Methyl-1,2,4-Triazole with Group IIIA Metal Halides. *Zh. Obshch. Khim.* **1981**, *51*, 629−636.
(15) Billes, F.; Endrédi, H.; Keresztury, G. Vibrational Spectroscopy of Triazoles and Tetrazole. *J. Mol. Struct.: THEOCHEM* **2000**, *530*, 183−200.
(16) Wright, C. J.; Smith, R. N.; Kroll, J. A.; Shipman, S. T.; Widicus Weaver, S. L. Extending the Millimeter/Submillimeter Wave Spectrum of Ground State Pyruvic Acid for Comparison to Astronomical Data. *ACS Earth Space Chem.* **2022**, *6*, 482−495.
(17) Tokaryk, D. W.; Crouse, J. G.; Kim, D. Synchrotron-Based Rotation-Vibration Spectroscopy of Imidazole. *J. Mol. Spectrosc.* **2022**, *387*, No. 111647.
(18) Kisiel, Z.; Pszczółkowski, L.; Medvedev, I. R.; Winnewisser, M.; De Lucia, F. C.; Herbst, E. Rotational Spectrum of *Trans*−*Trans* Diethyl Ether in the Ground and Three Excited Vibrational States. *J. Mol. Spectrosc.* **2005**, *233*, 231−243.
(19) Kisiel, Z.; Pszczółkowski, L.; Drouin, B. J.; Brauer, C. S.; Yu, S.; Pearson, J. C.; Medvedev, I. R.; Fortman, S.; Neese, C. Broadband Rotational Spectroscopy of Acrylonitrile: Vibrational Energies from Perturbations. *J. Mol. Spectrosc.* **2012**, *280*, 134−144.
(20) Pickett, H. M. The Fitting and Prediction of Vibration-Rotation Spectra with Spin Interactions. *J. Mol. Spectrosc.* **1991**, *148*, 371−377.
(21) Kisiel, Z. PROSPE—Programs for ROtational SPEctroscopy. http://info.ifpan.edu.pl/~kisiel/prospe.htm. (accessed July 2024).
(22) Frisch, M. J.; Trucks, G. W.; Schlegel, H. B.; Scuseria, G. E.; Robb, M. A.; Cheeseman, J. R.; Scalmani, G.; Barone, V.; Petersson, G. A.; Nakatsuji, H. et al. *Gaussian 16*, rev C.01; Gaussian, Inc.: Wallingford, CT, USA, 2016.
(23) Schmidt, J. R.; Polik, W. F. *WebMO Enterprise*, version 19.0; WebMO LLC: Madison, WI, USA, 2019 http://www.webmo.net. (accessed January 2023).
(24) Stanton, J. F.; Gauss, J.; Cheng, L.; Harding, M. E.; Matthews, D. A.; Szalay, P. G.; Auer, A. A.; Bartlett, R. J.; Benedikt, U.; Berger, C.; Bernholdt, D. E.; Bomble, Y. J.; Christiansen, O.; Engel, F.; Faber, R.; Heckert, M.; Heun, O.; Huber, C.; Jagau, T.-C.; Jonsson, D.; Jusélius, J.; Klein, K.; Lauderdale, W. J.; Lipparini, F.; Metzroth, T.; Mück, L. A.; O'Neill, D. P.; Price, D. R.; Prochnow, E.; Puzzarini, C.; Ruud, K.; Schiffmann, F.; Schwalbach, W.; Simmons, C.; Stopkowicz, S.; Tajti, A.; Vázquez, J.; Wang, F.; Watts, J. D.; CFOUR. Coupled-Cluster techniques for Computational Chemistry, a quantum-chemical program package. http://www.cfour.de. (accessed July 2024).
(25) Mills, I. M. Vibration-Rotation Structure in Asymmetric- and Symmetric-Top Molecules. In *Molecular Spectroscopy: Modern Research*; Rao, K. N.; Mathews, C. W., Eds.; Academic Press: New York, 1972; Vol. *1*, pp 115−140.
(26) Stanton, J. F.; Lopreore, C. L.; Gauss, J. The Equilibrium Structure and Fundamental Vibrational Frequencies of Dioxirane. *J. Chem. Phys.* **1998**, *108*, 7190−7196.
(27) Schneider, W.; Thiel, W. Anharmonic Force Fields from Analytic Second Derivatives: Method and Application to Methyl Bromide. *Chem. Phys. Lett.* **1989**, *157*, 367−373.
(28) Watson, J. K. G. Determination of Centrifugal Distortion Coefficients of Asymmetric-Top Molecules. *J. Chem. Phys.* **1967**, *46*, 1935−1949.
(29) Winnewisser, G. Millimeter Wave Rotational Spectrum of HSSH and DSSD. II. Anomalous *K* Doubling Caused by Centrifugal Distortion in DSSD. *J. Chem. Phys.* **1972**, *56*, 2944−2954.
(30) van Eijck, B. P. Reformulation of Quartic Centrifugal Distortion Hamiltonian. *J. Mol. Spectrosc.* **1974**, *53*, 246−249.
(31) Typke, V. Centrifugal Distortion Analysis Including P^6-Terms. *J. Mol. Spectrosc.* **1976**, *63*, 170−179.
(32) Margulès, L.; Perrin, A.; Demaison, J.; Merke, I.; Willner, H.; Rotger, M.; Boudon, V. Breakdown of the Reduction of the Rovibrational Hamiltonian: The Case of $S^{18}O_2F_2$. *J. Mol. Spectrosc.* **2009**, *256*, 232−237.
(33) Motiyenko, R. A.; Margulès, L.; Alekseev, E. A.; Guillemin, J. C.; Demaison, J. Centrifugal Distortion Analysis of the Rotational

https://doi.org/10.1021/acs.jpca.4c03890
J. Phys. Chem. A 2024, 128, 6927−6942

Spectrum of Aziridine: Comparison of Different Hamiltonians. *J. Mol. Spectrosc.* **2010**, *264*, 94−99.
(34) Barnum, T. J.; Lee, K. L. K.; McGuire, B. A. Chirped-Pulse Fourier Transform Millimeter-Wave Spectroscopy of Furan, Isotopologues, and Vibrational Excited States. *ACS Earth Space Chem.* **2021**, *5*, 2986−2994.
(35) Tokaryk, D. W.; Culligan, S. D.; Billinghurst, B. E.; van Wijngaarden, J. A. Synchrotron-Based Far-Infrared Spectroscopy of Furan: Rotational Analysis of the ν_{14}, ν_{11}, ν_{18} and ν_{19} Vibrational Levels. *J. Mol. Spectrosc.* **2011**, *270*, 56−60.
(36) Esselman, B. J.; Zdanovskaia, M. A.; Amberger, B. K.; Shutter, J. D.; Owen, A. N.; Billinghurst, B. E.; Zhao, J.; Kisiel, Z.; Woods, R. C.; McMahon, R. J. Millimeter-wave and High-Resolution Infrared Spectroscopy of the Low-Lying Vibrational States of Pyridazine Isotopologues. *J. Chem. Phys.* **2024**, *160*, No. 194301.

https://doi.org/10.1021/acs.jpca.4c03890
J. Phys. Chem. A 2024, 128, 6927−6942